

Lithium-intercalation-induced structural evolution and superconductivity modulation in 2H-Li*x*TaSe$_2$

Lijia Zhou(周立佳), Xiangjiang Dong(董祥江), Qiang Li(李强), Xiaojun Kuang(匡小军), and Xianran Xing(邢献然)
Citation: Chin. Phys. B, 2025, 34 (**11**): 117402. DOI: 10.1088/1674-1056/ade24f
http://cpb.iphy.ac.cn; http://iopscience.iop.org/cpb

What follows is a list of articles you may be interested in

Pressure-stabilized Li_2K electride with superconducting behavior

Xiao-Zhen Yan(颜小珍), Quan-Xian Wu(邬泉县), Lei-Lei Zhang(张雷雷), and Yang-Mei Chen(陈杨梅)
Chin. Phys. B, 2025, 34 (**9**): 097405. DOI: 10.1088/1674-1056/add009

Superconductivity and band topology of double-layer honeycomb structure M_2N_2 (*M* = Nb, Ta)

Jin-Han Tan(谭锦函), Na Jiao(焦娜), Meng-Meng Zheng(郑萌萌), Ping Zhang(张平), and Hong-Yan Lu(路洪艳)
Chin. Phys. B, 2025, 34 (**9**): 097402. DOI: 10.1088/1674-1056/adee04

Surface reconstruction modulated superconductivity on quasi-2D iron pnictide superconductor $KCa_2Fe_4As_4F_2$

Wenjing Zeng(曾文静), Zongyuan Zhang(张宗源), Xiaoyan Dong(董晓燕), Yubing Tu(涂玉兵), Yanwei Wu(吴彦玮), Teng Wang(王腾), Fan Zhang(张凡), Shuai Shao(邵帅), Jie Hou(侯杰), Xingyuan Hou(侯兴元), Ning Hao(郝宁), Gang Mu(牟刚), and Lei Shan(单磊)
Chin. Phys. B, 2025, 34 (**8**): 087402. DOI: 10.1088/1674-1056/add5cb

Superconductivity in YbN_4H_{12} under low pressures

Xiang Wang(汪翔), Chenlong Xie(谢晨龙), Haohao Hong(洪浩豪), Yanliang Wei(魏衍亮), Zhao Liu(刘召), and Tian Cui(崔田)
Chin. Phys. B, 2025, 34 (**8**): 087401. DOI: 10.1088/1674-1056/add908

Theoretical investigation of potential superconductivity in Sr-doped $La_3Ni_2O_7$ at ambient pressure

Lei Shi(石磊), Ying Luo(罗颖), Wei Wu(吴为), and Yunwei Zhang(张云蔚)
Chin. Phys. B, 2025, 34 (**7**): 077403. DOI: 10.1088/1674-1056/add1bd

---

Lithium-intercalation-induced structural evolution and superconductivity modulation in 2H-Li_xTaSe_2

Lijia Zhou(周立佳)[1], Xiangjiang Dong(董祥江)[2], Qiang Li(李强)[1], Xiaojun Kuang(匡小军)[3], and Xianran Xing(邢献然)[1,†]

[1] *Beijing Advanced Innovation Center for Materials Genome Engineering and Institute of Solid-State Chemistry, University of Science and Technology Beijing, Beijing* 100083, *China*

[2] *Center for High-Pressure Science and Technology Advanced Research, Beijing* 100093, *China*

[3] *Guangxi Key Laboratory of Electrochemical and Magnetochemical Functional Materials, College of Chemistry and Bioengineering, Guilin University of Technology, Guilin* 541004, *China*

(Received 6 May 2025; revised manuscript received 29 May 2025; accepted manuscript online 9 June 2025)

We systematically investigated the structural and superconducting properties of polycrystalline 2H-Li_xTaSe_2 ($0.1 \leq x \leq 1.0$) synthesized via a high-temperature solid-state reaction. Lithium (Li) intercalation induces an expansion along the *c*-axis and intralayer distortions within the Ta–Se coordination network. The superconducting transition temperature (T_c) is increased to 2.95 K at $x = 0.1$ driven by the synergistic enhancement of the electronic density of states at the Fermi level, $N(E_F)$, and strengthened electron–phonon coupling. With further Li doping, although $N(E_F)$ continues to increase, lattice stiffening and pronounced distortions in the Ta–Se coordination polyhedra weaken the electron–phonon interaction, ultimately suppressing superconductivity. These findings highlight the critical role of intralayer structural modulation in governing structure-tunable superconductivity in layered materials.

Keywords: superconductivity, Li intercalation, local structural distortion

PACS: 74.70.Ad, 74.62.Bf, 74.25.Dw

DOI: 10.1088/1674-1056/ade24f **CSTR:** 32038.14.CPB.ade24f

1. Introduction

Layered transition metal dichalcogenides (TMDCs) are an important class of quantum materials that exhibit rich electronic phenomena, including charge-density waves (CDWs) and superconductivity (SC), due to their low-dimensional structure and strong electron–phonon interactions. These materials adopt a layered crystal structure with the general formula MX_2, where M represents a transition metal (e.g., Ti, Zr, Hf, V, Nb, Ta, Mo, W, or Re), and X denotes a chalcogen element (S, Se, or Te).[1–3] Each MX_2 layer comprises a hexagonally arranged transition metal sheet sandwiched between two chalcogen layers, with adjacent layers held together by weak van der Waals forces. This structural feature not only gives rise to anisotropic electronic behavior but also enables intercalation of external atoms or molecules, offering an effective strategy for tuning the electronic structure and physical properties.[4–6] Due to these structural characteristics, TMDCs provide a versatile platform for exploring tunable correlated states, including CDWs and SC.

$TaSe_2$ is a representative member of the TMDC family, exhibiting multiple polymorphic structures, including 1T, 2H, 3R, 4H and 6R phases.[7] Specifically, 2H-$TaSe_2$ exhibits low-temperature superconductivity at approximately 0.14 K,[8] along with two characteristic CDW transitions: an incommensurate CDW at 120 K and a commensurate CDW at 90 K.[9–11] Previous studies have shown strong competition and mutual exclusivity between CDW order and the SC state. Experimental results indicate that applying external pressure effectively suppresses the CDW state, thereby enhancing the T_c to as high as 8.5 K.[12] Chemically, partial substitution of selenium with sulfur (e.g., in the $TaSe_{2-x}S_x$ system) can enhance T_c to around 2.5 K.[13] Furthermore, the intercalation of nonmagnetic elements (e.g., Cu, Ni, Pd, Pt, Sn, In, Pb)[14–20] expands the interlayer spacing and increases carrier concentration, thereby further enhancing its superconducting properties. Meanwhile, alkali metal intercalation, as an important tuning strategy, has shown significant potential in enhancing SC in various TMDCs. For example, $SnSe_2$ transforms from a semiconductor to a metal upon Li intercalation and exhibits superconductivity at low temperature.[21] In A_xTaS_2 (A = Li, Na, K, Rb, Cs) systems, intercalated alkali ions can enhance T_c up to 6 K.[22]

The influence of alkali metal intercalation on the 2H-$TaSe_2$ system has also been preliminarily investigated.[23–27] For instance, early studies employed n-butyllithium solution to intercalate Li into 2H-$TaSe_2$ single crystals, but the resulting 2H-$Li_{0.99}TaSe_2$ did not exhibit superconductivity.[24] In contrast, Wu *et al.* achieved controlled Li intercalation in two-dimensional 2H-$TaSe_2$ thin layers using a liquid electrolyte gating technique and successfully induced a superconducting

†Corresponding author. E-mail: xing@ustb.edu.cn

© 2025 Chinese Physical Society and IOP Publishing Ltd. All rights, including for text and data mining, AI training, and similar technologies, are reserved.

transition at around 2 K.[25] These findings suggest that the intercalation method and the resulting structural evolution have a significant impact on the superconducting properties, particularly in two-dimensional systems. In this study, we systematically investigate the effect of Li intercalation on the structure and superconducting properties of 2H-$TaSe_2$ over a broad doping range. Unlike previous studies that mainly focused on single crystal or low-dimensional systems, our approach in high-temperature solid-state synthesis enables precise control of Li content and comprehensive characterization of bulk physical properties. The observed non-monotonic dependence of T_c with Li doping is analyzed in terms of lattice distortion, electronic density of states, and electron–phonon coupling. Our findings provide new insights into structure-tunable superconductivity in TMDCs and may inspire further exploration of intercalation-driven quantum phase modulation in layered materials.

2. Experimental details

Polycrystalline 2H-Li_xTaSe_2 samples were synthesized via a high-temperature solid-state reaction. The starting materials (99.9% Li_2Se, 99.99% Ta, 99.9% Se powders) were weighed according to the stoichiometric ratio, mixed, ground, pelletized, and sealed in an evacuated quartz tube. Due to the volatility of Li and Se, 0.05 MPa of high-purity argon gas was introduced into the quartz tube prior to sealing, in order to suppress their evaporation. The sealed tube was subsequently placed in a muffle furnace and annealed at 800 °C for 12 hours. After annealing, the samples were cooled to room temperature in the furnace.

X-ray powder diffraction (XRPD) data were collected using a Rigaku SmartLab 9 kW diffractometer (Japan) with Cu $K\alpha$ radiation to examine the phase formation of the samples. X-ray photoelectron spectroscopy (XPS) measurements were performed using an EscalabXi + A9951381 spectrometer with Al $K\alpha$ x-ray radiation as the excitation source. The microstructure was examined using scanning electron microscopy (SEM) and energy-dispersive spectroscopy (EDS) for elemental mapping, performed using a Zeiss Gemini SEM 500. Electrical resistivity and thermal properties were measured using a physical property measurement system (PPMS, Quantum Design), with the resistivity determined using the standard four-probe method. Magnetization measurements were conducted using a magnetic property measurement system (MPMS, Quantum Design).

2.1. Results and discussion

Figure 1 illustrates the effect of Li intercalation on the crystal structure of 2H-$TaSe_2$. The phase composition and purity of the samples were characterized using XRPD data. As shown in Fig. 1, except for a small amount of Li_2Se impurity phase observed at high doping levels ($x = 0.8$–1), the XRPD patterns of other samples match well with the standard 2H-type structure, indicating the formation of a continuous solid solution over the Li concentration range of 0.1–0.7. The enlarged view on the right ($2\theta = 12°$–$15°$) further reveals a gradual shift of the (002) diffraction peak toward lower angles with increasing Li content, indicating successful intercalation of Li into the 2H-$TaSe_2$ structure. Figure 2(d) presents the Rietveld-refined XRPD pattern of the $x = 0.1$ sample, which shows good fitting quality ($R_{wp}/R_p = 5.64\%/4.28\%$), further confirming its high phase purity and structural order. Figures 2(a)–2(c) display the systematic evolution of lattice parameters with increasing Li content, extracted from Rietveld refinements of the XRPD data. As x increases, the unit cell volume expands significantly, with the c-axis lattice constant increasing from 12.9403(3) Å to 13.5787(4) Å and the a-axis increasing slightly from 3.4459(4) Å to 3.4703(3) Å. This trend is consistent with observations in other typical intercalated systems such as 2H-Cu_xTaSe_2[14] and 2H-Pd_xTaSe_2,[20] further confirming the effective interlayer intercalation of Li atoms.

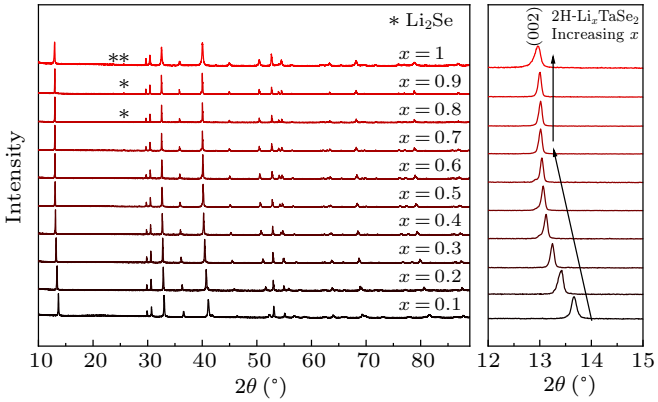


Fig. 1. XRPD patterns of 2H-Li_xTaSe_2 ($x = 0.1$–1). Peaks marked with ∗ indicate the presence of the Li_2Se impurity phase. The right panel shows an enlarged view of the (002) peak, which shifts to lower angles with increasing Li content x.

Figure 2(e) further illustrates the subtle effects of Li intercalation on the intralayer coordination geometry of $TaSe_2$, as revealed by bond lengths and bond angles obtained from Rietveld refinements of the XRPD data. As the Li content increases, the two characteristic Se–Ta–Se bond angles exhibit distinct trends. Angle 1 gradually increases and stabilizes, whereas angle 2 gradually decreases before reaching a plateau. This behavior suggests a c-axis elongation of the local coordination environment while preserving the overall intralayer symmetry. Moreover, the Ta–Se bond lengths increase continuously with rising Li intercalation levels, suggesting that intercalation modulates the local bonding strength. The spacing between the top and bottom Se atomic layers is also stretched, further confirming the elastic response of the crystal structure

along the interlayer (c-axis) direction. Previous studies employing ^{181}Ta Mössbauer spectroscopy have shown that Li intercalation partially reduces Ta^{4+} ions to nearly Ta^{3+}, indicating electron donation from Li to the $TaSe_2$ host lattice, manifesting as typical n-type carrier doping.[27] This electron injection process is accompanied by weak coordination or ionic interactions between Li and Se atoms, which drives the systematic evolution of lattice parameters.[25,27]

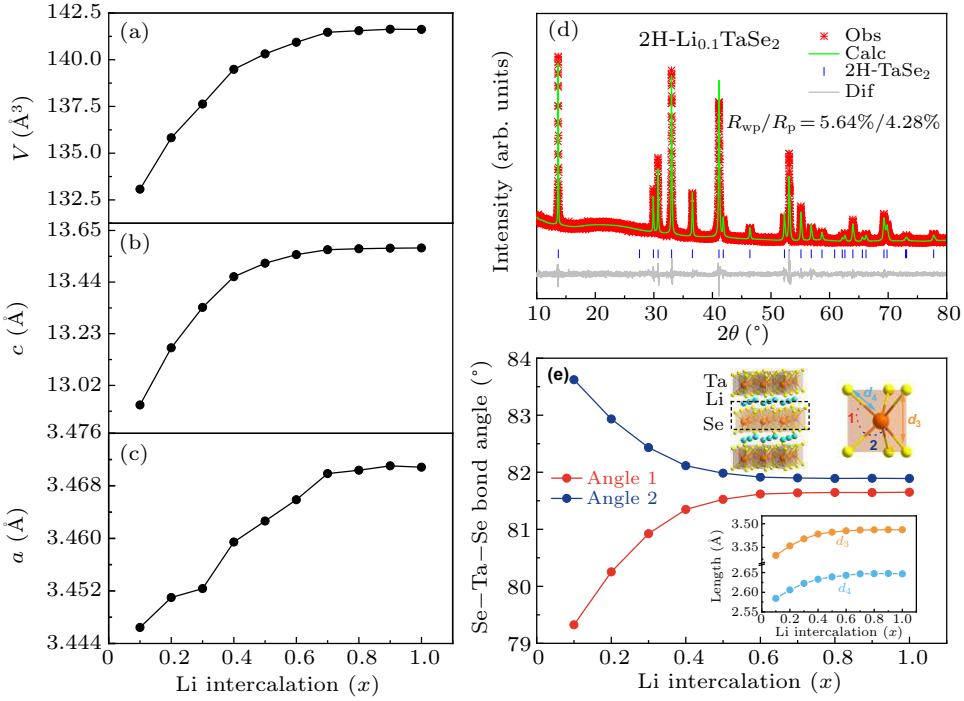


Fig. 2. (a)–(c) The evolution of lattice parameters V, c, and a with increasing Li content. (d) Rietveld refinement of XRPD data for 2H-$Li_{0.1}TaSe_2$. (e) The effects of Li intercalation on the intralayer coordination geometry of $TaSe_2$. The inset illustrates the crystal structure and intralayer coordination unit of 2H-Li_xTaSe_2, along with changes in Ta–Se bond lengths and the interlayer spacing between the two Se atomic planes.

The effects of Li intercalation on CDW and SC were investigated using systematic resistivity measurements. Figure 3(a) presents the temperature-dependent normalized resistivity for 2H-Li_xTaSe_2 ($0.1 \leq x \leq 1$) samples. As the Li content increases from 0.1 to 1, the low-temperature normalized resistivity gradually decreases, while the residual resistivity ratio (RRR) increases significantly. These results suggest that Li intercalation effectively enhances the metallic behavior of the system and reduces carrier scattering at low temperatures. No signatures of CDW phase transitions were observed across the entire temperature range, suggesting that Li intercalation likely weakens or fully suppresses CDW formation.[25] Figure 3(b) provides a magnified view highlighting the superconducting transition in 2H-Li_xTaSe_2. With increasing Li content, T_c increases sharply from the reported value of ~ 0.14 K in pristine 2H-$TaSe_2$,[8] reaching 2.95 K at $x = 0.1$ and 2.65 K at $x = 0.2$, before gradually declining and eventually vanishing at higher doping levels. Figure 3(c) presents the magnetic susceptibility curves of 2H-Li_xTaSe_2 ($x = 0.1$ and 0.2) measured under ZFC and FC conditions with an external magnetic field of 10 Oe. Low-field magnetization measurements confirm the presence of bulk superconductivity in the 2H-Li_xTaSe_2 system. The trend of T_c with Li content is consistent with the resistivity measurements. Additionally, similar enhancements in superconductivity have been reported in 2H-$TaSe_2$ through intercalation with other elements in different systems.[14–17,19,20]

To determine the upper critical field (H_{c2}), the temperature-dependent resistivity of the 2H-$Li_{0.1}TaSe_2$ sample was measured under various applied magnetic fields, as shown in Fig. 4(a). The T_c at each field was determined using the 90% normalized resistivity criterion. The relationship between H_{c2} and T_c is illustrated in Fig. 4(b). By fitting the experimental data using the Ginzburg–Landau (G-L) model $H_{c2} = H_{c2}(0)[1-(T/T_c)^2]/[1+(T/T_c)^2]$, the zero-temperature upper critical field $H_{c2}(0)$ for 2H-$Li_{0.1}TaSe_2$ was estimated to be 9.89 T.

The isothermal magnetization (M–H) curves of 2H-$Li_{0.1}TaSe_2$ at various temperatures are presented in Fig. 4(c). The lower critical field (H_{c1}) was determined by identifying the deviation point from the initial linear Meissner response in the isothermal magnetization curves. Figure 4(d) presents the temperature dependence of H_{c1}. By fitting the data using the G-L model $H_{c1} = H_{c1}(0)[1-(T/T_c)^2]$, the zero-temperature lower critical field $H_{c1}(0)$ was estimated to be 42.49 mT.

A range of superconducting parameters (Table 1) can be derived from the $H_{c2}(0)$ and $H_{c1}(0)$ values. According to the relevant equation $H_{c2}(0) = \Phi_0/(2\pi\xi^2)$, the G-L coherence length (ξ) of 2H-$Li_{0.1}TaSe_2$ is estimated as 5.77 nm, with Φ_0 denoting the flux quantum. The magnetic penetration depth (λ) is calculated using the equation $H_{c1}(0) =$

$\Phi_0/(4\pi\lambda^2)(\ln k)$, where $k = \lambda/\xi$ denotes the G-L parameter. The obtained λ and k are 44 nm and 7.62, respectively. Since k is much larger than $1/\sqrt{2}$, this indicates that 2H-$Li_{0.1}TaSe_2$ is a type-II superconductor.

The low-temperature specific heat for the 2H-Li_xTaSe_2 ($x = 0.1, 0.2$) samples is presented in Fig. 5. Notably, the C_p/T versus T exhibits pronounced peaks at $T_c \approx 2.95$ K ($x = 0.1$) and 2.65 K ($x = 0.2$), consistent with the resistivity and magnetization measurements, further confirming the presence of bulk superconductivity. After subtracting the phonon contribution, the electronic specific heat component of the $x = 0.1$ sample was extracted (see the inset of Fig. 5). Based on the Bardeen–Cooper–Schrieffer (BCS) model, the jump in electronic specific heat was determined to be $\Delta C_e/\gamma T_c = 1.44$, which is close to the weak-coupling limit predicted by the BCS theory. This result indicates that 2H-Li_xTaSe_2 is a typical weak-coupling superconductor.

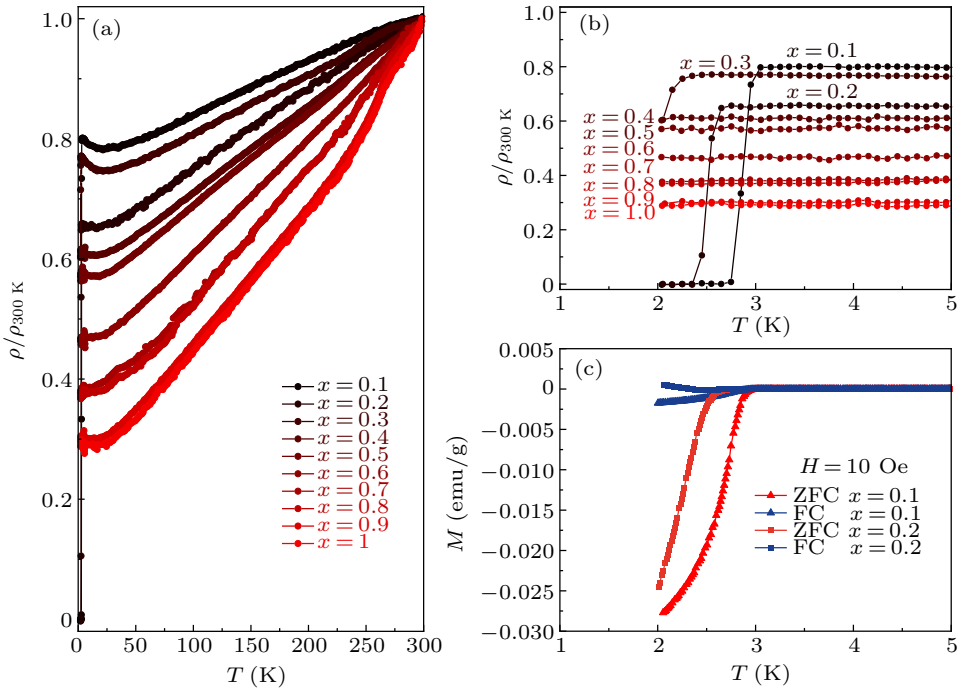


Fig. 3. (a) The temperature dependence of normalized resistivity $\rho/\rho_{300\ K}$ for 2H-Li_xTaSe_2 ($x = 0.1$–1). (b) An enlarged view of the normalized resistivity $\rho/\rho_{300\ K}$ in the low-temperature range of 1–5 K. (c) The temperature dependence of magnetic susceptibility for 2H-Li_xTaSe_2 ($x = 0.1$ and 0.2) measured under $H = 10$ Oe in zero-field-cooled (ZFC) and field-cooled (FC) modes.

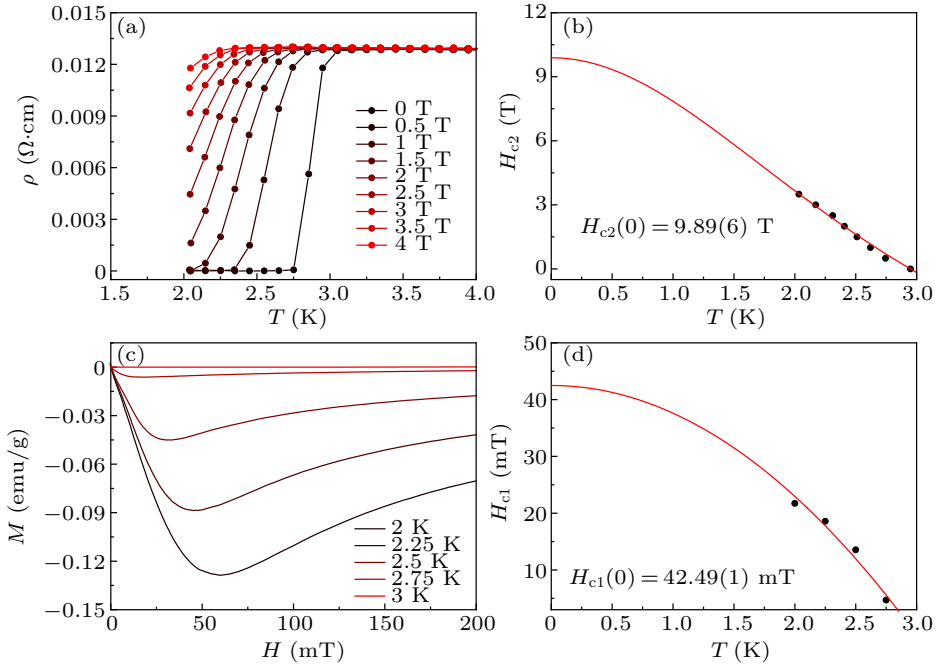


Fig. 4. (a) The temperature dependence of the resistivity of 2H-$Li_{0.1}TaSe_2$ under various magnetic fields. (b) The temperature dependence of the upper critical field H_{c2} for 2H-$Li_{0.1}TaSe_2$. (c) Field-dependent magnetization measured at various temperatures for 2H-$Li_{0.1}TaSe_2$. (d) The temperature dependence of the lower critical field H_{c1} for 2H-$Li_{0.1}TaSe_2$.

Table 1. Superconducting parameters of 2H-$Li_{0.1}TaSe_2$.

Parameter	Unit	2H-$Li_{0.1}TaSe_2$
T_c	K	2.95
H_{c1}	mT	42.49
H_{c2}	T	9.89
ξ	nm	5.77
λ	nm	44
κ		7.62
γ	mJ·mol^{-1}·K^{-2}	9.73
β	mJ·mol^{-1}·K^{-4}	0.91
Θ_D	K	184.80
λ_{ep}		0.67
$\Delta C_e/\gamma T_c$		1.44

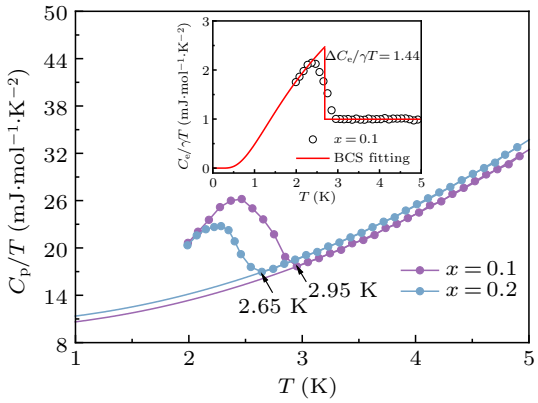


Fig. 5. (a) The temperature dependence of specific heat C_p/T for 2H-Li_xTaSe_2 ($x = 0.1$ and 0.2) samples. The inset shows the electronic specific heat C_e/T at the optimal intercalation level ($x = 0.1$). The red dashed line represents a fit to the superconducting state using a single-gap BCS model.

The normal-state specific heat between T_c and 5 K can be fitted using the expression $C_p/T = \gamma + \beta T^2$, where the γ and β represent the electronic and phonon specific heat coefficients, respectively. The results show that as the Li content increases from $x = 0.1$ to 0.2, the γ value increases from 9.72 mJ·mol^{-1}·K^{-2} to 10.43 mJ·mol^{-1}·K^{-2}, indicating a higher electronic density of states at the Fermi level $N(E_F)$. The Debye temperature (Θ_D) is related to β through the expression $\Theta_D = (12\pi^4 RN/5\beta)^{1/3}$, where N is the number of atoms per formula unit and R is the gas constant. As the Li content increases, the β decreases from 0.91 mJ·mol^{-1}·K^{-4} to 0.88 mJ·mol^{-1}·K^{-4}, while the Θ_D increases from 184.80 K to 187.07 K, indicating a slight increase in lattice stiffness and suggesting lattice hardening.

The extended Eliashberg theory[28] and its corresponding semi-empirical McMillan formula[29] suggest that the T_c is closely related to the electron–phonon coupling constant (λ_{ep}), Θ_D and $N(E_F)$. The λ_{ep} can be calculated using the McMillan formula

$$\lambda_{ep} = \frac{1.04 + \mu^* \mathrm{In}\left(\frac{\Theta_D}{1.45T_c}\right)}{(1 - 0.62\mu^*)\mathrm{In}\left(\frac{\Theta_D}{1.45T_c}\right) - 1.04}.$$

Assuming a Coulomb pseudopotential μ^* of 0.15, the estimated λ_{ep} are approximately 0.67 ($x = 0.1$) and 0.65 ($x = 0.2$). Based on the parameters λ_{ep} and γ, $N(E_F)$ was calculated using the standard expression $N(E_F) = 3\gamma/(\pi^2 k_B^2(1 + \lambda_{ep}))$, yielding values of 2.48 and 2.71 states·eV^{-1} for $x = 0.1$ and $x = 0.2$. The obtained values of λ_{ep} and $N(E_F)$ are significantly higher than those of pristine 2H-$TaSe_2$ ($\lambda_{ep} \approx 0.4$),[20] and are comparable to those reported for metal-intercalated systems such as 2H-Cu_xTaSe_2,[14] 2H-Ni_xTaSe_2,[15] and 2H-Pb_xTaSe_2.[20] These findings suggest that in the low-doping regime, the enhancement of T_c in the 2H-Li_xTaSe_2 system is mainly attributed to the increased λ_{ep} and $N(E_F)$.

However, with further increases in Li content, although the $N(E_F)$ continues to rise, the λ_{ep} does not increase accordingly and instead shows a slight decline, leading to a downward trend in T_c. In 2D systems, Li intercalation via ionic liquid gating has been shown to enhance T_c from 0.14 K to $\sim$2 K, despite a reduced carrier concentration and a transition from a multiband to a single-band Fermi surface. This behavior is primarily attributed to the suppression of the CDW order and the associated disappearance of soft phonon modes, which significantly enhances electron–phonon interactions. In contrast, the bulk 2H-Li_xTaSe_2 samples exhibit a more pronounced lattice response to Li intercalation, particularly in the form of c-axis expansion and intralayer coordination unit distortions. To better understand this behavior, the potential mechanisms underlying the decrease in λ_{ep} were further analyzed based on the Eliashberg theory $\lambda_{ep} = N(E_F)\langle I^2\rangle/(M\langle\omega^2\rangle)$.[28] On the one hand, Li intercalation leads to lattice stiffening, which increases the average phonon frequency $\langle\omega^2\rangle$ and thereby weakens the electron–phonon coupling strength. On the other hand, local structural distortions may disrupt existing coupling channels or reduce the matrix element $\langle I^2\rangle$, further weakening the effective λ_{ep}. As a result of the combined effects of these two mechanisms, T_c exhibits a decreasing trend despite the enhanced $N(E_F)$, due to the disruption of the electron–phonon coupling mechanism.

To systematically reveal the differences in superconducting behavior induced by different intercalation pathways, the key superconducting parameters (T_c, γ, Θ_D, λ_{ep} and $N(E_F)$) of several metal-intercalated 2H-$TaSe_2$ and 2H-TaS_2 compounds were collected and compared, with the data summarized in Table 2. In typical metal-intercalated systems (e.g., Pd, Ni, Cu),[5,14,15,30–32] the introduction of d-orbital electrons and activation of low-frequency vibrational modes during intercalation usually lead to simultaneous increases in λ_{ep} and $N(E_F)$, thereby effectively enhancing T_c. A similar enhancement in superconductivity is also observed in the Li-intercalated 2H-TaS_2 system,[33] where T_c reaches approximately 3.5 K around $x = 0.096$ before slightly decreasing. This enhancement is

attributed to the synergistic effect of CDW suppression and increased $N(E_F)$. Structural characterizations reveal that the crystal structure retains the 2H phase without significant distortion, thereby preserving electron–phonon coupling channels and enabling sustained enhancement of superconductivity.

Table 2. Superconducting parameters of various intercalated TMDCs.

Compound	T_c (K)	γ (mJ·mol^{-1}·K^{-2})	Θ_D (k)	λ_{ep}	$N(E_F)$ (states·eV^{-1})	References
2H-TaS_2	0.8	8	165	0.52*	2.23*	[30]
2H-$Pd_{0.04}TaS_2$	4.2	16.84	208.5	0.73	4.14	[31]
2H-$Ni_{0.04}TaS_2$	4.15	13.02	244.7*	0.69*	3.27*	[32]
2H-$Cu_{0.04}TaS_2$	4.5	12	165	0.8*	2.85*	[30]
2H-$Li_{0.096}TaS_2$	3.5	11.2	245	0.65	3.04*	[33]
2H-$TaSe_2$	0.14	5	202	0.4	1.51	[20]
2H-$Pd_{0.09}TaSe_2$	3.3	8.5	196	0.67	2.16	[20]
2H-$Ni_{0.02}TaSe_2$	2.7	8.13	196	0.65	2.09	[15]
2H-$Cu_{0.07}TaSe_2$	2.7	8.56	178.8	0.657	2.2	[14]
2H-$Li_{0.1}TaSe_2$	2.95	9.72	184.80	0.67	2.47	this work
2H-$Li_{0.2}TaSe_2$	2.65	10.43	187.07	0.65	2.71	this work

The calculated parameters derived from the data presented in Refs. [30–33] are denoted by *.

The Li-intercalated 2H-$TaSe_2$ material exhibits a T_c enhancement trend similar to that of the aforementioned systems in the low-doping regime. However, at higher doping levels, its superconducting behavior then deviates significantly. Specifically, after an initial increase, T_c decreases sharply and eventually vanishes at $x = 0.3$. This phenomenon is closely related to c-axis expansion and intralayer coordination distortion induced by intercalation, suggesting that local structural perturbations and increased lattice stiffness play a dominant role in modulating the electron–phonon coupling mechanism and ultimately destabilize the superconducting state. This transition from cooperative enhancement to superconductivity suppression highlights the profound impact of structural perturbations on electron–phonon coupling and superconducting behavior in TMDCs, offering new insights into the design of tunable layered superconductors.

3. Conclusion

In conclusion, our results reveal a non-monotonic evolution of superconductivity in 2H-Li_xTaSe_2 induced by Li intercalation, governed by the interplay between enhanced electron–phonon coupling and intercalation-induced structural distortions. The superconducting transition temperature T_c reaches a maximum of 2.95 K at $x = 0.1$, driven by both the strengthened coupling strength and increased $N(E_F)$. However, further Li doping induces lattice stiffening and intralayer coordination distortions, and ultimately suppresses superconductivity despite continued carrier injection. These findings underscore the dominant role of structural modulation in determining the superconducting behavior, and provide valuable insights into intercalation-driven phase tuning in low-dimensional quantum systems.

Acknowledgement

This research was supported by the National Natural Science Foundation of China (Grant Nos. 22090042 and 22175018).

References

[1] Wilson J A, Di Salvo F and Mahajan S 1975 *Adv. Phys.* **24** 117
[2] Wilson J A and Yoffe A 1969 *Adv. Phys.* **18** 193
[3] Rossnagel K 2011 *J. Phys. Condens. Matter* **23** 213001
[4] Morosan E, Zandbergen H W, Dennis B, Bos J, Onose Y, Klimczuk T, Ramirez A, Ong N and Cava R J 2006 *Nat. Phys.* **2** 544
[5] Morosan E, Wagner K E, Zhao L L, Hor Y, Williams A J, Tao J, Zhu Y and Cava R J 2010 *Phys. Rev. B* **81** 094524
[6] Gamble F, DiSalvo F, Klemm R and Geballe T 1970 *Science* **168** 568
[7] Katzke H, Tolédano P and Depmeier W 2004 *Phys. Rev. B* **69** 134111
[8] Van Maaren M and Schaeffer G 1967 *Phys. Lett. A* **24** 645
[9] Moncton D, Axe J and DiSalvo F 1975 *Phys. Rev. Lett.* **34** 734
[10] Moncton D E, Axe J and DiSalvo F 1977 *Phys. Rev. B* **16** 801
[11] Fleming R, Moncton D, McWhan D and DiSalvo F 1980 *Phys. Rev. Lett.* **45** 576
[12] Freitas D, Rodière P, Osorio M, Navarro-Moratalla E, Nemes N, Tissen V, Cario L, Coronado E, García-Hernández M and Vieira S 2016 *Phys. Rev. B* **93** 184512
[13] Li L, Deng X, Wang Z, Liu Y, Abeykoon M, Dooryhee E, Tomic A, Huang Y, Warren J B and Bozin E S 2017 *npj Quantum Mater.* **2** 11
[14] Li X, Zhou M, Yang L and Dong C 2017 *Supercond. Sci. Technol.* **30** 125001
[15] Li L, Sun Y, Zhu X, Wang B, Zhu X, Yang Z and Song W 2010 *Solid State Commun.* **150** 2248
[16] Lawan Adam M, Buba Garba I, Alhaji Bala A, Aji Suleiman A, Muhammad Gana S and Lawan Adam F 2023 *Phys. Rev. B* **107** 104510
[17] Adam M L, Liu Z, Moses O A, Wu X and Song L 2021 *Nano Res.* **14** 2613
[18] Ali M N, Gibson Q D, Klimczuk T and Cava R J 2014 *Phys. Rev. B* **89** 020505
[19] Li Y, Wu Y, Xu C, Liu N, Ma J, Lv B, Yao G, Liu Y, Bai H and Yang X 2021 *Sci. Bull.* **66** 243
[20] Bhoi D, Khim S, Nam W, Lee B, Kim C, Jeon B G, Min B, Park S and Kim K H 2016 *Sci. Rep.* **6** 24068
[21] Wu H, Li S, Susner M, Kwon S, Kim M, Haugan T and Lv B 2019 *2D Materials* **6** 045048

[22] Lerf A, Sernetz F, Biberacher W and Schöllhorn R 1979 *Mater. Res. Bull.* **14** 797

[23] Brauer H, Starnberg H, Holleboom L, Hughes H and Strocov V 2001 *J. Phys. Condens. Matter* **13** 9879

[24] Murphy D W, Di Salvo F J, Hull Jr G W and Waszczak J V 1976 *Inorg. Chem.* **15** 17

[25] Wu Y, Xing H, Lian C S, Lian H, He J, Duan W, Liu J, Mao Z and Liu Y 2019 *Phys. Rev. Mater.* **3** 104003

[26] König A, Koepernik K, Schuster R, Kraus R, Knupfer M, Büchner B and Berger H 2012 *Europhys. Lett.* **100** 27002

[27] Eibschutz M, Salomon D, Murphy D, Zahurak S and Waszczak J 1987 *Chem. Phys. Lett.* **135** 591

[28] Allen P B and Mitrović B 1983 *Solid State Phys.* **37** 1

[29] McMillan W L 1968 *Phys. Rev.* **167** 331

[30] Wagner K, Morosan E, Hor Y, Tao J, Zhu Y, Sanders T, McQueen T, Zandbergen H, Williams A and West D 2008 *Phys. Rev. B* **78** 104520

[31] Zhou M, Li X and Dong C 2018 *Supercond. Sci. Technol.* **31** 065001

[32] Zhu X, Sun Y, Zhang S, Lei H, Li L, Zhu X, Yang Z, Song W and Dai J 2009 *Solid State Commun.* **149** 1296

[33] Liu H, Huangfu S, Zhang X, Lin H and Schilling A 2021 *Phys. Rev. B* **104** 064511